RSC Advances

PAPER

Cite this: *RSC Adv.*, 2020, **10**, 323

Aqueous-based electrospun P(NIPAAm-*co*-AAc)/RSF medicated fibrous mats for dual temperature- and pH-responsive drug controlled release†

Juan Li, Jingxin Zhu, * Lan Jia, Yanlong Ma and Haijuan Wu

Received 28th October 2019
Accepted 17th December 2019

DOI: 10.1039/c9ra08832f

rsc.li/rsc-advances

This paper presents a green method for fabricating dual temperature- and pH-responsive electrospun fibrous mats from an aqueous-based blend poly(*N*-isopropylacrylamide-*co*-acrylic acid) (P(NIPAAm-*co*-AAc)) and regenerated silk fibroin (RSF) by employing electrospinning technique. P(NIPAAm-*co*-AAc) was synthesized by free radical solution polymerization and its low critical solution temperature (LCST) was in the physiological range (38.8 °C). The P(NIPAAm-*co*-AAc)/RSF fibers were prepared by electrospinning technology in the presence of the crosslinking agents (EDC·HCl and NHS) with water as solvent. After *in situ* crosslinking and water-annealing process, the water-stable composite fibrous mats were obtained. Scanning electron microscopy (SEM) and Fourier transform infrared spectroscopy (FTIR) were used to analyze the crosslinking process. Temperature and pH dual stimuli-responsive swelling-shrinking behavior of the fibrous mats were observed when the temperature was below and above the LCST of the copolymer at different pHs. In addition, rhodamine B-loaded the fibrous mats also showed dual temperature and pH controlled release behavior, demonstrating the potential use of the fibrous mats for "smart" controlled drug delivery applications.

Introduction

"Smart" or stimuli-responsive polymers respond to small changes in their environment, such as temperature, pH, ionic strength, or light *etc.*, by markedly changing their chemical and physical properties. These polymers have been intensively studied due to their promising applications in drug delivery, tissue engineering, catalyst carrier and biosensors.[1–6]

Among the "Smart" polymers, temperature-responsive polymers respond to changes in the temperature and undergo a phase transition at the lower critical solution temperature (LCST). At temperatures below the LCST, these macromolecules are hydrophilic, while at temperatures above LCST, they become hydrophobic and collapse.[7] Poly(*N*-isopropylacrylamide) (PNIPAAm) is one of the most popular temperature-sensitive polymers,[8,9] and its LCST is around 32 °C. In order to raise the LCST of PNIPAAm to make it closer to the physiological temperature of the human body, NIPAAm can be copolymerized with hydrophilic monomers. This can be attributed to the formation of intrachain hydrogen bonds between the two groups, hydrophilic monomer and NIPAAm.[10,11] Acrylic acid (AAc) is a kind of hydrophilic monomer which can be copolymerized with NIPAAm to obtain poly(*N*-isopropylacrylamide-*co*-acrylic acid) P(NIPAAm-*co*-AAc).[12] Due to its molecular structure contains temperature-sensitive amide group and pH-sensitive carboxyl group, the LCST of P(NIPAAm-*co*-AAc) can be adjusted depending to the change of composition, meanwhile, the copolymer has the characteristic of dual response of temperature and pH, which has a good application prospect in the field of drug carriers.[13,14]

Responsive drug carriers come in various forms, such as hydrogels,[15,16] microgels,[17] films[18] and macro-nanofibers.[19–21] The form of macro-nanofibers have uniquely advantage because the features provide extremely large surface area and porosity, which enhance the sensitivity to external stimuli.[22] Electrospinning is the most facile, convenient and effective method to produce micro and nano-fibrous mats.[23,24] A variety of nanostructured fibers can be prepared by several kinds of electrospinning processes, such as 2-fluid coaxial,[25] side-by-side,[26] and other complex electrospinning processes.[27] In recent years, the related work of the electrospinning PNIPAAm as temperature responsive fiber carriers have been published,[28–32] but there are a limited number of studies concerning temperature and pH dual-stimuli responsive systems of P(NIPAAm-*co*-AAc), moreover, most of these systems were processed into hydrogels and nanoparticles.[33–35] This is because preparing water-stable P(NIPAAm-*co*-AAc) nanofibers is a quite challenging task when the temperature of aqueous media is lower than LCST. Generally, the method of preparing water-insoluble fibers is post-treatment crosslinking, which can be physical or chemical crosslinking. For example, NIPAAm had to be copolymerized with crosslinkable monomers (NMA) to achieve water-insoluble electrospun fibers by a heat induced chemical crosslinking.[36] For

College of Materials Science and Engineering, Taiyuan University of Technology, Taiyuan, 030024, China. E-mail: zhujingxin@tyut.edu.cn

† Electronic supplementary information (ESI) available: Characterization of P(NIPAAm-*co*-AAc); DSC curves of fibrous mats; *in vitro* drug release study. See DOI: 10.1039/c9ra08832f

P(NIPAAm-*co*-AAc) copolymer, because it contains a small number of carboxyl groups in the macromolecules structure, chemical crosslinking can be achieved by bioconjugation reaction between carboxyl groups and amino groups with the assistance of crosslinking agent. Commonly crosslinking agents are glutaraldehyde, genipin, 1-ethyl-3-(3-dimethylaminopropyl) carbodiimide (EDC), *etc.*, among them, the EDC is higher the crosslinking efficiency when it combined with *n*-hydroxysuccinimide (NHS). Adamsen and co-workers had successfully fabricated *in situ* crosslinked PNIPAM/gelatin nanofibers by electrospining PNIPAM–NHS and gelatin in the presence of the crosslinking agents EDC and NHS.[37] Lin and co-workers[38] obtained a stimuli-responsive electrospun composite nanofibers from P(NIPAAm-*co*-AAc) and polyurethane (PU) blends. However, due to the use of DMF organic solvent in the preparation process, it would raise safety concerns when it applied to drug carrier and tissue engineering.

Regenerated silk fibroin (RSF), extracted from *Bombyx mori* cocoons, is a protein polymer which has good biocompatibility and biodegradation and has been successfully used as drug delivery systems in various forms, such as nanospheres, films and nanofibers.[39–43] Mixing RSF with P(NIPAAm-*co*-AAc) is expected to improve the biocompatibility and biodegradability of P(NIPAAm-*co*-AAc)-based materials, which is accordant with the economic friendly and green development strategy.

The aim of the present study was to developed a green method for fabricating temperature and pH dual-stimuli responsive fibrous mats by using electrospinning technique from P(NIPAAm-*co*-AAc) and RSF blends. In brief, firstly, P(NIPAAm-*co*-AAc) copolymer was synthesized by free radical solution polymerization, and then the composite fibers of P(NIPAAm-*co*-AAc)/RSF were prepared by electrospinning technology combined with *in situ* crosslinking and with water as solvent. Moreover, after water-annealing process, the insolubility of the composite fibrous mats was further improved, which was due to the physical crosslinking of RSF in composite fiber. Finally, rhodamine B was selected as a model drug and encapsulated in composite fibers and the drug release behavior of the fibrous mats at different temperatures and pHs were investigated.

Experimental section

Materials

N-Isopropylacrylamide (NIPAAm), *N*-hydroxysuccinimide (NHS) and *N*-(3-dimethylaminopropyl)-*N*′-ethylcarbodiimide hydrochloride (EDC·HCl) were purchased from Aladdin Chemistry Co., Ltd. (Shanghai, China). The NIPAAm monomer was recrystallized from methylbenzene/*n*-hexane, and 2,2′-azobis(isobutyronitrile) (AIBN) was recrystallized from ethanol. Cocoons of *Bombyx mori* were purchased from Zhejiang, China. All reagents such as acrylic acid (AAc), LiBr, and rhodamine B were of analytical grade, and used as received without further purification.

Synthesis of P(NIPAAm-*co*-AAc) copolymers of different composition

Copolymers were synthesized by free radical solution polymerization using ethanol as solvent shown in Scheme 1(a). Reactions were performed in a round bottom flask. Firstly, NIPAAm and AAc, with a molar ratio of NIPAAm : AAc = 100 : 0, 100 : 8, 100 : 12 or 100 : 20, were dissolved in ethanol and initiator, AIBN, 0.2 mol% to the amount of NIPAAm was added. After that, nitrogen was bubbled through the solution for 30 min and then started the reactions. The polymerizations were performed at 70 °C for 24 h in N_2 atmosphere. Afterward the polymer was precipitated in diethyl ether by adding the solution dropwise and purified twice washing steps. Finally, the polymer was isolated by filtration and vacuum-dried for 24 h.

Preparation of regenerated silk fibroin (RSF) aqueous solution

RSF aqueous solution was prepared according to previously described procedure.[44] In brief, cocoons were cut into small pieces and were boiled twice for 30 min in a 0.5 wt% Na_2CO_3 solution, then rinsed with deionized water at 60 °C to remove the residual sericin. After drying at ambient conditions overnight, the degummed fibers were dissolved in a 9.3 M LiBr solution at 60 °C for 2 h. After filtration, the silk solution was dialyzed against deionized water for 3 days with dialysis tubing (MWCO 14 000 ± 8000 Da) to remove salts. Finally, the solution was concentrated by forced airflow to produce a 30 wt% RSF aqueous solution.

Electrospinning for P(NIPAAm-*co*-AAc)/RSF fibers and crosslinking

The preparation procedure of P(NIPAAm-*co*-AAc)/RSF fibers is as follows. Firstly, preparation of the different ratios of P(NIPAAm-*co*-AAc) and RSF aqueous-based spinning solutions contained the crosslinking agents (EDC·HCl and NHS) and rhodamine B.

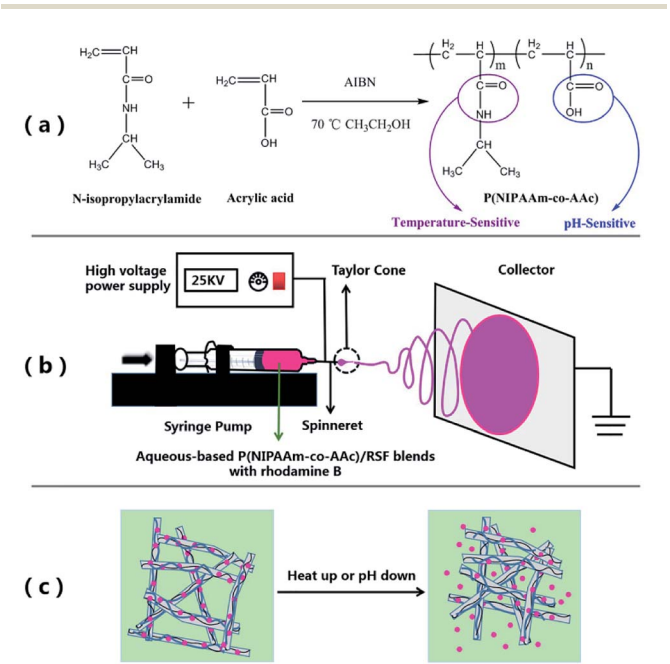

Scheme 1 Schematic of (a) synthesis of P(NIPAAm-*co*-AAc), (b) electrospinning of aqueous-based P(NIPAAm-*co*-AAc)/RSF blends with rhodamine B and (c) rhodamine B stimuli-responsive release from P(NIPAAm-*co*-AAc)/RSF fibers.

Table 1 Preparation of aqueous-based P(NIPAAm-*co*-AAc)/RSF spinning solution with different ratios of P(NIPAAm-*co*-AAc) and RSF which contained EDC·HCl, NHS and rhodamine B

Solution	Amount of P(NIPAAm-*co*-AAc) (wt%)	Amount of RSF (wt%)	Mass ratios of P(NIPAAm-*co*-AAc) and RSF (wt/wt)	EDC·HCl (wt%)	NHS (wt%)	Rhodamine B (wt%)	Surface tension (mN m^{-1})
a	20	30	1 : 1	10	10		58.513
b	22	30	1 : 1	10	10		43.035
c	24	30	1.5 : 1 (15.7%)[a]	10	10	0.2	44.240
d	24	30	1 : 1 (13.3%)[a]	10	10	0.2	41.366
e	24	30	1 : 1.5 (10.9%)[a]	10	10	0.2	36.071
f	26	30	1 : 1	10	10		40.161

[a] The concentration of P(NIPAAm-*co*-AAc) in P(NIPAAm-*co*-AAc)/RSF blended solution, wt%.

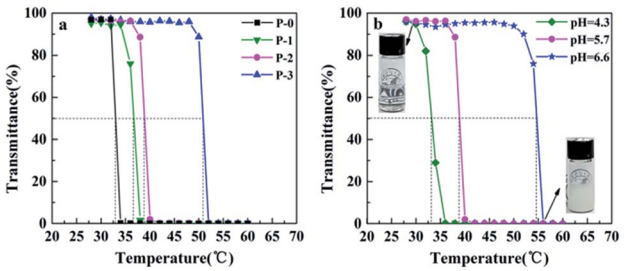

Fig. 1 Variation in the transmittance at 500 nm of 1 wt% P(NIPAAm-*co*-AAc) in PB aqueous solution with temperature: (a) different AAc content at pH 5.7, (b) copolymer P-2 at different pHs.

Table 1 shows the composition of the mixtures which named solution a–f. All the solutions were mixed at room temperature until the copolymer, crosslinking agent and drug were completely dissolved. Secondly, electrospinning: the P(NIPAAm-*co*-AAc)/RSF aqueous-based spinning solution was loaded into the 10 mL syringe fitted with a 21 G steel needle as a spinneret. The syringe was mounted on a horizontal syringe pump (RWD 202, RWD Life Science Co., Ltd). The fibers were prepared by applying a voltage of 25 kV, a flow rate of 0.5 mL h^{-1}, and the distance between the tip of needle and the collector is 15 cm. The electrospinning process shows in Scheme 1(b). Finally, crosslinking of the P(NIPAAm-*co*-AAc)/RSF as-spun fibers: the as-spun fibers containing the EDC·HCl and NHS were placed in a vacuum oven of 45% humidity for 3 days to induce *in situ* crosslinkage of P(NIPAAm-*co*-AAc) with RSF, after that, the water-annealing process was applied to the *in situ* crosslinked fibers. The fibers were put the vacuum oven which a water-filled plate in the bottom chamber at 75 °C for 1 h at 90% RH to promote the conformational transformation of RSF.

Characterization

Fourier transform infrared spectra (FTIR) were recorded on a Tensor II Spectrometer (Bruker, Germany) with a resolution of 4 cm^{-1} over the wavenumber range from 400–4000 cm^{-1}. ^{1}H NMR spectra were measured by a Avance III 400 MHz spectrometer (Bruker, Germany) and DMSO-d_6 was used as the solvent. The gel permeation chromatography (GPC) measurements were performed on a 1515 instrument (Waters, America) equipped Waters 4.6 × 30 mm guard column and DMF (containing 50 mmol L^{-1} LiBr) as the eluent at 35 °C with a flow rate of 1 mL min^{-1}, PMMA was used as standard. The LCST of the copolymer was defined as the temperature at which transmittance of the solution decreased in 50% using a SQ-2800 UV-vis Spectrophotometer (UNICO, China). Before the measurement, the PNIPAAm or P(NIPAAm-*co*-AAc) was dissolved in phosphate buffer saline (PB, pH 5.7) to prepare 1 wt% solution, meanwhile, the copolymer solutions of the same concentration in PB (pH 4.3, 5.7 and 6.6) were prepared for the study of the LCSTs of the copolymer. The morphology of P(NIPAAm-*co*-AAc)/RSF fibers were observed with a Mira 3 scanning electron microscopy (SEM), (TESCAN, Czech). Digital photographs were taken to illustrate the crosslinking of P(NIPAAm-*co*-AAc)/RSF fibers. The contact angles of the P(NIPAAm-*co*-AAc)/RSF fibrous mats at different temperature and pH, and the surface tension of spinning solutions were determined on the JC2000D1 measuring instrument (Shanghai Powereach, China).

Table 2 Polymerization conditions, molecular weight, and LCSTs of P(NIPAAm-*co*-AAc) copolymers

Sample	Feeding ratio NIPAAm : AAc (mol mol^{-1})	Composition ratio NIPAAm : AAc[a] (mol mol^{-1})	M_w[b] (g mol^{-1})	PDI[b]	LCST (°C) pH 5.7	LCST (°C) pH 6.6
P-0	100 : 0	100 : 0			32.9	32.9
P-1	100 : 8	100 : 11			36.5	45.4
P-2	**100 : 12**	**100 : 16**	**6.6 × 10^4**	**1.57**	**38.8**	**54.6**
P-3	100 : 20	100 : 24			50.8	

[a] Determined by ^{1}H NMR. [b] Determined by GPC.

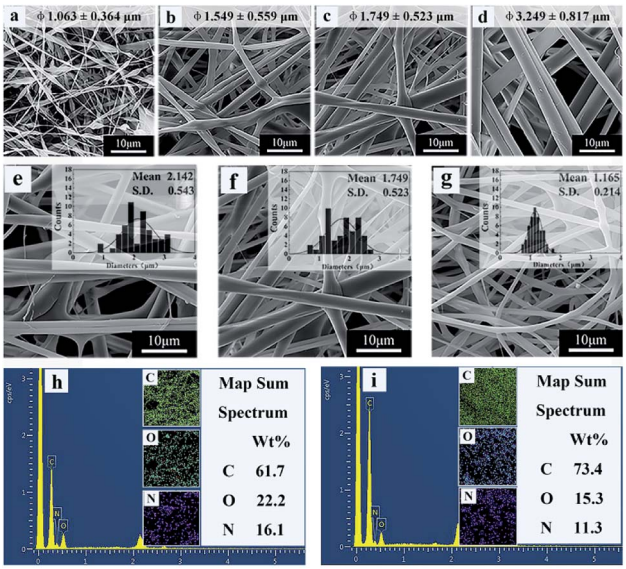

Fig. 2 SEM images of electrospun P(NIPAAm-*co*-AAc)/RSF fibers: (a)–(d), the fibers fabricated from P(NIPAAm-*co*-AAc)/RSF blended solutions with the mass ratio of copolymer and RSF is 1 : 1, but the initial concentrations of P(NIPAAm-*co*-AAc) is 20, 22, 24 and 26 wt%, respectively. (e–g) The fibers fabricated from the different mass ratio of copolymer and RSF solutions with the content of P(NIPAAm-*co*-AAc) from 15.7, 13.3 to 10.9 wt%, respectively. (h and i) Element mapping images of P(NIPAAm-*co*-AAc)/RSF with the content of P(NIPAAm-*co*-AAc) 13.3 wt%, and P(NIPAAm-*co*-AAc), respectively.

The drug loaded fibers were observed using fluorescence microscope (Motic AE31, Beijing Ruikezhongyi Technology Co., Ltd) under phase contrast and fluorescence mode to detect the rhodamine B-stained.

In vitro drug release

For *in vitro* drug release test, 13 mg rhodamine B-loaded fibrous mat samples were immersed in a 10 mL tube containing 6 mL PB buffer (pH 5.7 or 6.6) and the solutions with samples were shaken at 60 rpm on a DKZ-2 orbital rotator (Yiheng, China) at 25, 40 and 60 °C, respectively. At predetermined times, 2 mL of solutions were taken out and 2 mL fresh PB buffer solution at the same pH was added to maintain the same total solution volume. The concentration of rhodamine B was measured through a SQ-2800 UV-vis (UNICO, China) at 554 nm, and then, eqn S1 and Fig. S6 in ESI Appendix† were used to calculate cumulative drug release. All drug release studies were carried out in triplicate.

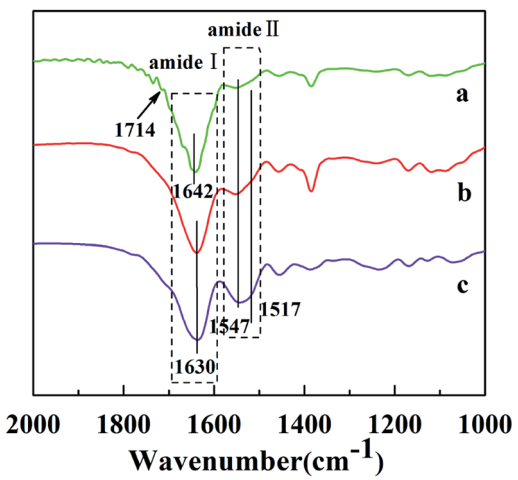

Fig. 3 FTIR spectra of P(NIPAAm-*co*-AAc)/RSF fibers: (a) as-spun fibers (b) *in situ* crosslinking fibers (c) after water-annealing of *in situ* crosslinking fibers.

Results and discussion

Synthesis and characterization of P(NIPAAm-*co*-AAc) copolymers

P(NIPAAm-*co*-AAc) copolymers of different composition named P-0, P-1, P-2, P-3 shown in Table 2 were synthesized by free radical solution polymerization in ethanol with AIBN as initiator. The prepared random copolymers were identified by ^{1}H NMR and FTIR. In the ^{1}H NMR spectrum of P(NIPAAm-*co*-AAc) copolymer, the proton signals of the NIPAAm moiety are observed at peaks 1.0 (–CH_3), 3.81 (–CH) and 7.16 (–NH) ppm, respectively, while the peak related to AAc moiety is at 11.97 (–COOH) ppm. In addition, the copolymer main chain proton signals are shown at 1.41–1.94 ppm. The NIPAAm/AAc composition of copolymers estimated from the ratio on the area integration of the peak at 7.16 (–NH) with at 11.97 (–COOH) and the results are shown in Table 2. In the FTIR spectrum of copolymer P-2, the peaks at 1650 and 1550 cm^{-1} are assigned to C=O bending and N–H stretching, respectively. The broad

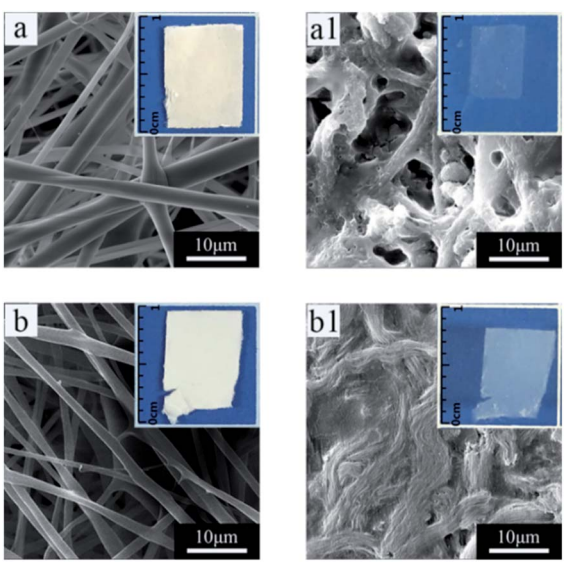

Fig. 4 SEM images and digital photos of *in situ* crosslinked P(NIPAAm-*co*-AAc)/RSF fibrous mats before and after water-annealing: (a) dried fibrous mats before water-annealing, (a1) wetted fibrous mats before water-annealing immersed in PB solution with a pH of 5.7 at 25 °C, and (b) dried fibrous mats after water-annealing, (b1) wetted fibrous mats after water-annealing immersed in PB solution with a pH of 5.7 at 25 °C.

absorption band at around 3300–3400 cm^{-1} is assigned to the N–H stretching, the peaks at 1368 cm^{-1} and 1386 cm^{-1} are arisen from the stretching of the $-CH(CH_3)_2$ groups in NIPAAm. The peaks at 1715 cm^{-1} is assigned to the C=O stretching of carboxylic group of AAc units. The details of ^1H NMR and FTIR spectrum are shown in Fig. S1 and S2 in ESI Appendix.† Thus, the P(NIPAAm-*co*-AAc) copolymer have been successfully synthesized *via* the radical copolymerization.

The weight average molecular weight (M_w), and PDI (M_w/M_n) of copolymer P-2 calculated from GPC is 6.6×10^4 and 1.57 (the GPC curve is displayed in Fig. S3 in ESI Appendix†).

The phase-transition behaviors and LCSTs of the P(NIPAAm-*co*-AAc) copolymers in aqueous solutions were characterized by monitoring the change in light transmittance. The temperature at 50% of the initial transmittance was defined as the LCST. Fig. 1 shows variation in the transmittance at 500 nm of 1 wt% P(NIPAAm-*co*-AAc) in PB aqueous solution with temperature. The LCST of the copolymer (P-1, P-2 and P-3) increases from 36.5 to 50.8 °C with the increase of the content of AAc in the copolymer at pH 5.7 (Fig. 1a or Fig. S4 in ESI Appendix†), which are slightly higher than that of PNIPAAm with 32 °C, due to the hydrophilic characteristic of AAc units. Meanwhile, the copolymer P-2 exhibits pH-sensitive behaviors, the LCST increases with the increase of the pH value (Fig. 1b), due to the increase in the hydrophilicity of the AAc units caused by the hydrolysis increases of the copolymer with the increase of pH value.[7]

In particular, the LCST of copolymer P-2 at pH 5.7 is 38.8 °C, close to the physiological temperature of human body. Therefore, copolymer P-2 was selected for following studies.

Morphology of P(NIPAAm-*co*-AAc)/RSF fibers

The electrospinning process is influenced by many factors, resulting in different fiber morphology. The literatures reported that the solution concentration and surface tension have important effects on the morphology and diameter of the fibers.[45,46] In this work, spinning solutions with different mass ratio of copolymer and RSF named solution a–f were prepared according to the composition in Table 1 and the corresponding fibrous mats named sample a–f. Fig. 2 shows the morphology and diameter distribution of electrospun fibers fabricated from different ratios of P(NIPAAm-*co*-AAc) and RSF. At low initial concentrations of the copolymer (20 wt%), the fibers exhibit a "beads-on-a-string" morphology, with increase in the initial ratio of P(NIPAAm-*co*-AAc) in the P(NIPAAm-*co*-AAc)/RSF blended solution from 22 to 26 wt%, the beadless, uniform and stable flat ribbons fibers can be obtained (Fig. 2a–d). This is because the surface tension of the solution reduces (Table 1), which improves the stability of the jet of polymer solution, and favors formation of fibers without beads.[45] Therefore, 22 wt% is the lower boundary concentration of the P(NIPAAm-*co*-AAc) in the P(NIPAAm-*co*-AAc)/RSF blended solution in the case of the spinning parameters constant.

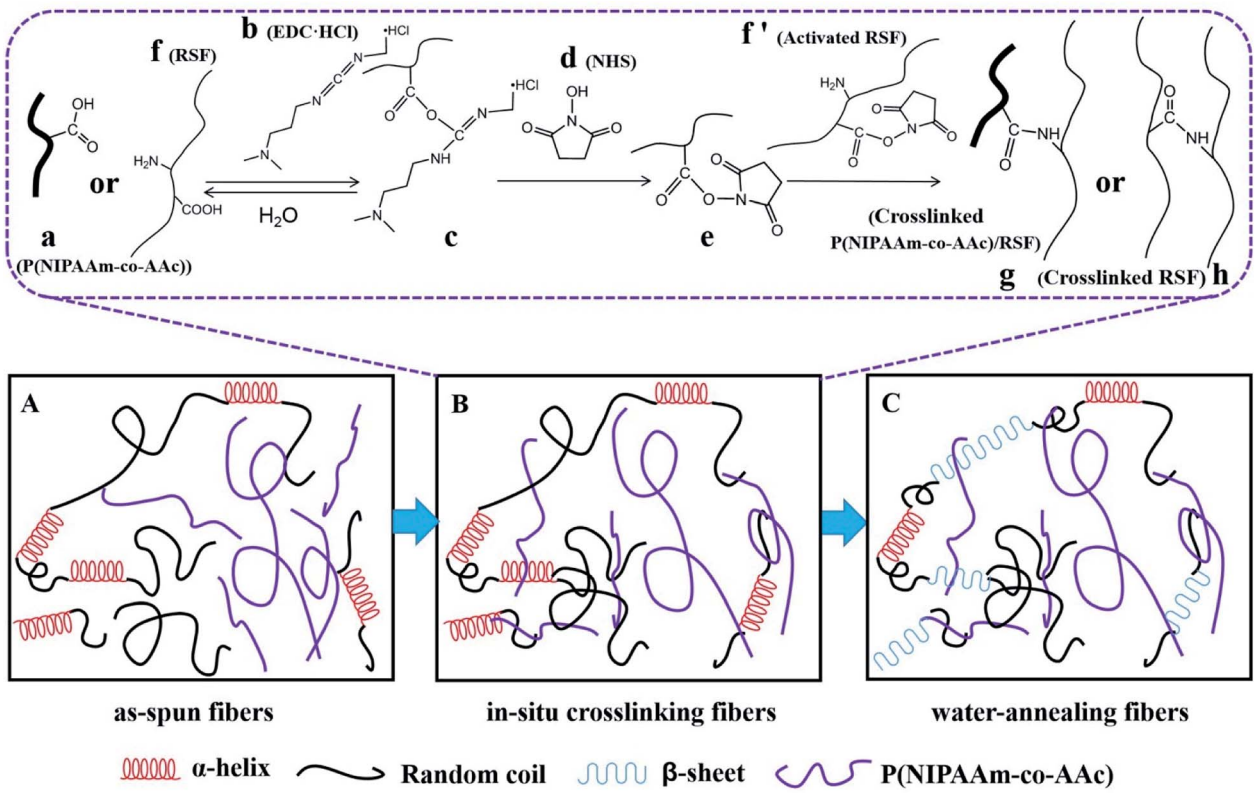

Fig. 5 Schematic mechanisms of *in situ* crosslinking and water-annealing of P(NIPAAm-*co*-AAc)/RSF fibers: (A) as-spun fibers, (B) *in situ* crosslinking fibers, (C) after water-annealing of *in situ* crosslinking fibers.

Fig. 2e–g show the fibers fabricated from the different mass ratios of P(NIPAAm-*co*-AAc) and RSF solutions with the content of P(NIPAAm-*co*-AAc) from 15.7, 13.3 to 10.9 wt%, respectively. With decrease the content of P(NIPAAm-*co*-AAc) in the P(NIPAAm-*co*-AAc)/RSF blends, the morphology of the fibers is changed from flat ribbons into approximate cylindrical and the average diameter of the fibers is decreased from 2.142 ± 0.543 to 1.165 ± 0.214 μm.

This phenomenon can be attributed to the different volatilization of solvents in the spinning solution. The solvent in the spinning solution is water, and there are strong hydrogen bonds between the copolymer and water which results in the low volatility of residual solvent in the spinning jet and the production of ribbon fibers with larger diameter. When the content of copolymer in spinning solution decrease, the water is easy to volatilize and the morphology of the fibers is changed from flat ribbons into approximate cylindrical, meanwhile, the diameters of the fibers decreased. This finding is similar to that of Rockwood *et al.*[46]

Fig. 2h and i show the elemental mapping images of P(NIPAAm-*co*-AAc)/RSF fibers and P(NIPAAm-*co*-AAc) fibers. The contents of C, O and N of P(NIPAAm-*co*-AAc)/RSF fibers are 61.7%, 22.2% and 16.1%, respectively (Fig. 2h). Compared with pure P(NIPAAm-*co*-AAc) fibers (Fig. 2i), the content of C decreases and the content of O and N increases in P(NIPAAm-*co*-AAc)/RSF fibers. This is due to the high proportion of amino acids in the composition of RSF, which indicates that RSF has been evenly mixed with P(NIPAAm-*co*-AAc) in the fibers.

Crosslinking of P(NIPAAm-*co*-AAc)/RSF as-spun fibers

The as-spun fibers of P(NIPAAm-*co*-AAc)/RSF were soluble in water when the temperature was lower than LCST. In order to realize stable of the as-spun fibers, this work adopted two steps of crosslinking: *in situ* crosslinking and water-annealing process. *In situ* crosslinked P(NIPAAm-*co*-AAc)/RSF fibers were produced by chemical crosslinking between P(NIPAAm-*co*-AAc) and RSF with the help of EDC·HCl and NHS when the as-spun fibers had experienced a longer storage time, and water-annealing process could induce physical crosslinking through the conformational transformation of RSF. Fig. 3 shows FTIR spectra of P(NIPAAm-*co*-AAc)/RSF fibers at different crosslinking stages. In the spectrum of as-spun fibers, the peak of 1714 cm^{-1} is assigned to the C=O stretching of carboxylic group of AAc (Fig. 3a). As the *in situ* crosslinking occurred, the peak of 1714 cm^{-1} disappears and the peak of 1642 cm^{-1} corresponding to amide I (C=O) is shifted to 1630 cm^{-1}, indicating the occurrence of crosslinking. In addition, the DSC curve of P(NIPAAm-*co*-AAc)/RSF fibrous mats (Fig. S5 in ESI Appendix†) shows the thermal decomposition temperature of the fibrous mats increases after crosslinking process.

The reaction of *in situ* crosslinking could be explained in Fig. 5B: P(NIPAAm-*co*-AAc) (a) or RSF (f) are activated by EDC·HCl (b) to get the intermediate (c), however, intermediate (c) is unstable which is easy to hydrolyze into (a) or (f), so the introduction of the NHS (d) makes the unstable intermediates into stable intermediates (e), (e) with (f′) are aminated to realize the crosslinking between the copolymer and RSF (g) or RSF and RSF (h).[47]

The water-solubility of the fibers after *in situ* crosslinking was reduced (Fig. 4a1), however, when the fibrous mats were immersed into PB buffer solution at temperature lower than LCST, it still had a large volume reduction and the morphology of single fiber almost lost (Fig. 4a and a1), indicating that the fibrous mats was insufficient crosslinking. After water-annealing of *in situ* crosslinking fibers, the stability of the fibrous mats were improved, and the fiber basically maintained its morphology (Fig. 4b and b1). By comparing the FTIR spectra of before and after water-annealing of *in situ* crosslinking fibers (Fig. 3b and c), it can be found that the peak of 1547 cm^{-1} corresponding to amide II (α-helix and random coil conformation of RSF) is slight shifted to 1517 cm^{-1} (β-sheet conformation of RSF), meanwhile, the peak of 1630 cm^{-1} corresponding to amide I (β-sheet conformation of RSF) is also existence further indicating that water-annealing process can induced the conformation transformation of RSF from α-helix and random coil conformation to β-sheet conformation.[48] The crosslinking mechanisms of P(NIPAAm-*co*-AAc)/RSF fibers are shown in Fig. 5.

Temperature- and pH-dual stimuli-responsive behaviors of the fibrous mats

Stimuli-response behaviors of the fibers at different temperature and pH are the swelling and shrinkage, and resulting in changes in fiber diameter. These changes can be reflected by the

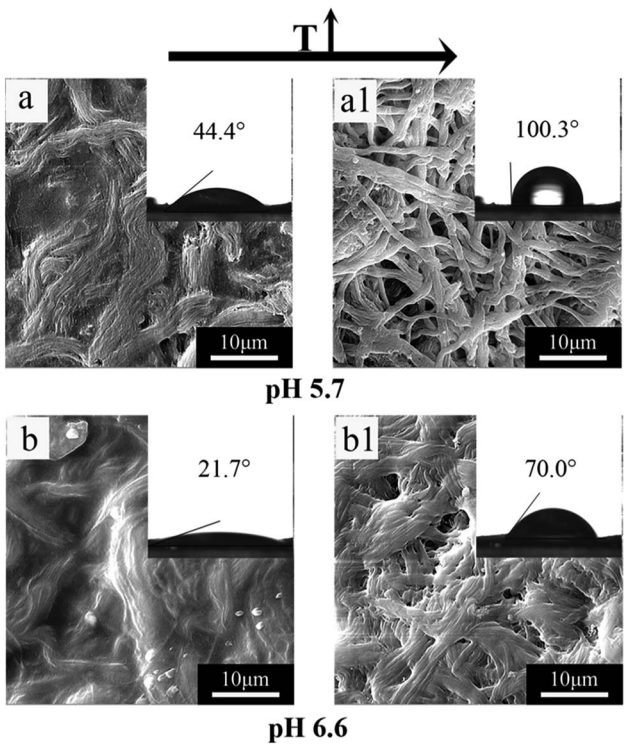

Fig. 6 SEM images and contact angle photos of P(NIPAAm-*co*-AAc)/RSF fibers at different temperatures and pHs: (a) the fibrous mats in PB solution with a pH of 5.7 at 25 °C, (a1) the fibrous mats in PB solution with a pH of 5.7 at 40 °C; (b) the fibrous mats in PB solution with a pH of 6.6 at 25 °C, (b1) the fibrous mats in PB solution with a pH of 6.6 at 40 °C.

morphology and contact angle values of fibrous mats. Fig. 6 shows the SEM images and contact angle photos of P(NIPAAm-*co*-AAc)/RSF fibrous mats at different temperatures and pH. Comparing Fig. 6a and a1 or Fig. 6b and b1, the composite fibers exhibit swelling and shrinkage behaviors when the temperature of PB solution increases from 25 to 40 °C. At room temperature (25 °C), the composite fibrous mats are hydrophilic corresponding with contact angle 44.4 or 21.7° respectively. At higher temperature (40 °C > LCST), the composite fibrous mats turn relatively hydrophobic exhibiting contact angles with 100.3° or 70.0°, which reflects temperature-responsive behavior of the composite fibers. Comparing Fig. 6a and b or Fig. 6a1 and b1, the composite fibers also exhibits swelling behaviors when the pH of PB solution increases from 5.7 to 6.6. At pH 5.7, the contact angle of the composite fibrous mats is 44.4 or 100.3°, at pH 6.6, the contact angle of the composite fibrous mats is 21.7 or 70.0°, the hydrophilic of the composite fibrous mats increases with the pH of PB solution from 5.7 to 6.6, which reflects pH-responsive behavior of the composite fibers. Based on the above data, P(NIPAAm-*co*-AAc)/RSF fibers have temperature- and pH-dual stimuli-responsive behaviors.

In vitro drug release behavior of fibers

Rhodamine B was chosen as model drug to be encapsulated during the one-step electrospinning process. Fig. 7 shows phase-contrast and fluorescent images of drug-loaded P(NIPAAm-*co*-AAc)/RSF fibers. The red fluoresce from rhodamine B (Fig. 7b) suggests rhodamine B exist in the fibers.

To investigate the temperature sensitivity of the fibrous mats, the temperature of *in vitro* drug release study were chosen 25 °C (<LCST), 40 °C (>LCST, close to the body temperature), and 60 °C (>LCST). Fig. 8 shows the release profiles of drug-release P(NIPAAm-*co*-AAc)/RSF fibrous mats at different temperature, pH and the content of P(NIPAAm-*co*-AAc) in fibrous mats. Fig. 8a presents rhodamine B release behaviors of P(NIPAAm-*co*-AAc)/RSF fibrous mats (sample d) in PB solution with a pH of 5.7 at different temperature. It can be seen that the cumulative release amount of rhodamine B increases from 56%, 68% to 74% with the increase of temperature from 25, 40 to 60 °C after the release process of 110 h, which shows temperature-dependent responsive release behavior. Due to the LCST of P(NIPAAm-*co*-AAc)/RSF

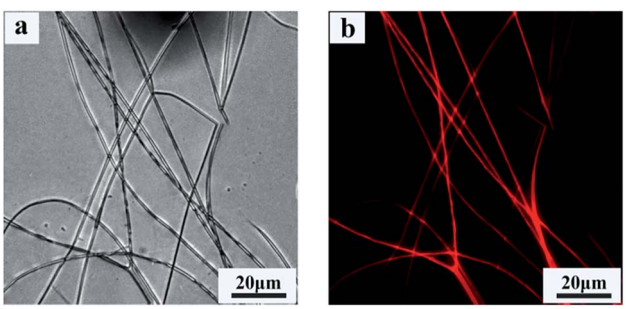

Fig. 7 Phase-contrast and fluorescent images of rhodamine B-loaded P(NIPAAm-*co*-AAc)/RSF fibers. (a) Phase-contrast image, (b) fluorescent image.

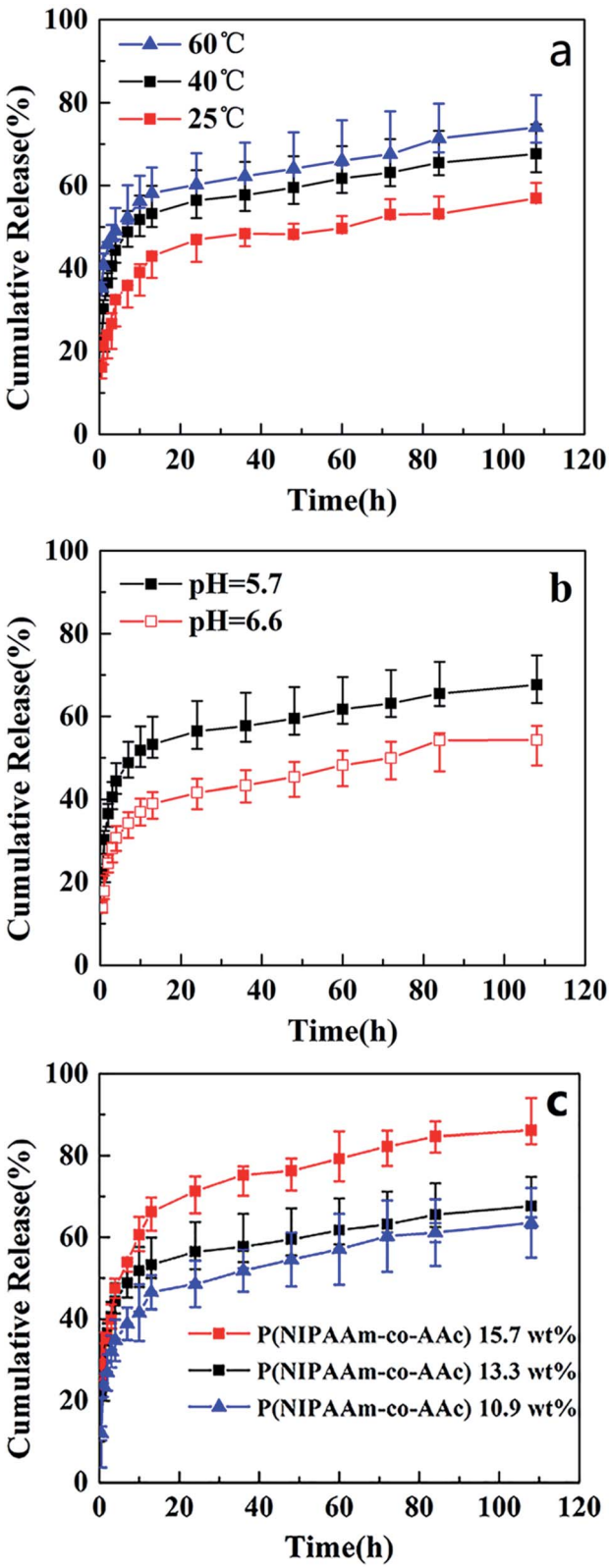

Fig. 8 The release profiles of rhodamine B-loaded P(NIPAAm-*co*-AAc)/RSF fibrous mats: (a) the fibrous mats (sample d) in PB solution with a pH of 5.7 at different temperature, (b) the fibrous mats (sample d) in PB solution with different pH at 40 °C, (c) The fibrous mats (sample c, d and e) fabricated from P(NIPAAm-*co*-AAc)/RSF solutions with the content of P(NIPAAm-*co*-AAc) from 15.7, 13.3 to 10.9 wt% respectively, in PB solution with a pH of 5.7 at 40 °C.

fibrous mats (copolymer P-2) is 38.8 °C, a small amount of rhodamine B are released into release medium at 25 °C. When the temperature rises to 40 °C (>LCST), the hydrogen bonds between P(NIPAAm-*co*-AAc) chains (–COOH with –COOH, –COOH with –NHCO, –NHCO with –NHCO) increase which lead to hydrophobic,[13] the fibers would shrink (Fig. 6a1), and rhodamine B is squeezed then released into PB solution, resulting the increase of accumulative release. When the temperature rises to 60 °C, the number of intrachain hydrogen bonds increases, resulting in a higher accumulative release.

Fig. 8b presents rhodamine B release behaviors of the fibrous mats (sample d) in PB solution with different pH at 40 °C. It shows that the release amount of rhodamine B decreases from 68% to 53% with the increase of pH from 5.7 to 6.6 after the release process of 110 h, indicating a pH-dependent responsive release behavior. The is because the carboxyl group (–COOH) in AAc unit of P(NIPAAm-*co*-AAc) chains is more easily ionized in the media environment of pH 6.6 than pH 5.7, it forms relatively more hydrogen bonds with water, resulting its hydrophilicity and swelling degree increase. Therefore, compared with the release amount of the fibrous mats at pH 5.7, which driven mainly by the shrinkage of the fibers, the that of fibrous mats decreases somewhat at pH 6.6.

In addition, Fig. 8c presents rhodamine B release behaviors of different content of P(NIPAAm-*co*-AAc) in the fibrous mats (sample c, d and e) immersed it in PB solution with a pH of 5.7 at 40 °C. It can be seen that the cumulative release amount of rhodamine B decreases from 86%, 68% to 62%, with the content of P(NIPAAm-*co*-AAc) decreases from 15.7, 13.3 to 10.9 wt% respectively, after the release process of 110 h, which shows P(NIPAAm-*co*-AAc) content-dependent responsive release behavior. Because the lower content P(NIPAAm-*co*-AAc) in the fibers, the lower sensitive the fibers is to the change of external environment, that is, the lower intermolecular hydrogen bonding of the P(NIPAAm-*co*-AAc) chains, which lead to the weaker shrinkage of the composite fibers, and the lower amount of rhodamine B are released. Schematic diagram of the controlled release of the rhodamine B-loaded fibrous mats at different temperature and pH is shown in Fig. 9.

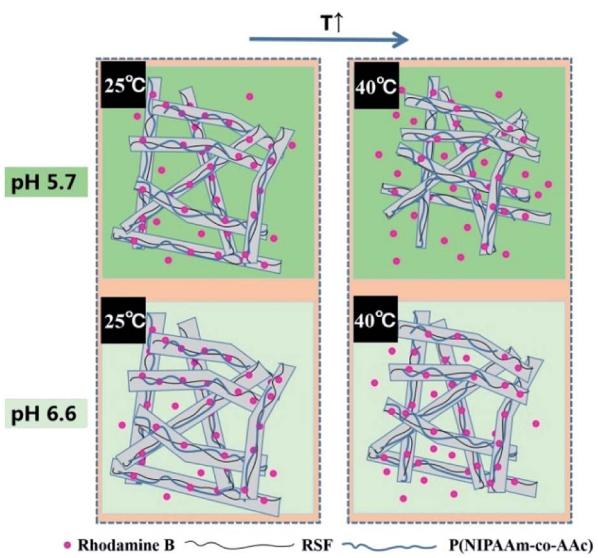

Fig. 9 Schematic diagram of the controlled release of rhodamine B-loaded P(NIPAAm-*co*-AAc)/RSF fibers at different temperature and pH.

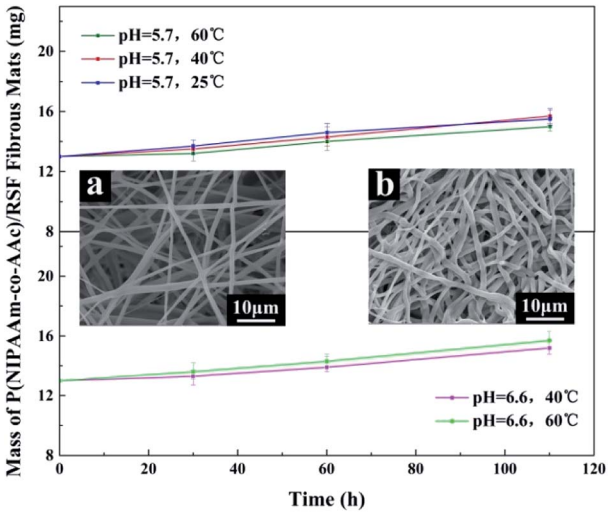

Fig. 10 The mass changes of P(NIPAAm-*co*-AAc)/RSF fibrous mats over time during drug release at variable temperature and pH conditions. And SEM images of fibrous mats: (a) before drug release; (b) after release 110 h.

To investigate the stability of P(NIPAAm-*co*-AAc)/RSF fibrous mats during drug release, we took out the fibrous mats at different times and weighed them after drying for 24 hours. Fig. 10 shows that the fibrous mats have good stability, and there is a slight increase in mass due to water absorption and swelling. Meanwhile, SEM images (Fig. 10a and b) shows that the surface of the fibers is smooth and no holes before and after drug release, which also proved the water-stability of the fibrous mats.

Conclusions

In this work, P(NIPAAm-*co*-AAc) copolymers were successfully synthesized and blended with RSF to create dual temperature- and pH-responsive of fibrous mats *via* electrospinning technique. The LCST of the copolymer increased with the increase of AAc unit content in the copolymer and could be adjusted close to human body temperature. Beadless, uniform as-spun fibers could be successfully produced by electrospinning from aqueous-based the copolymer and RSF blends in the presence of the crosslinking agents (EDC·HCl and NHS). After *in situ* crosslinking and water-annealing process, the water-stable fibrous mats were obtained. SEM images, FTIR and DSC were used to analyze the crosslinking process. Temperature and pH dual stimuli-responsive swelling-shrinking behavior of the fibrous mats were observed by SEM images and contact angle measurement when the temperature of PB solution was below and above the LCST of the copolymer at different pHs. Finally, rhodamine B-loaded the fibrous mats also showed dual temperature and pH controlled release behavior. Based on the above characteristics and the biocompatibility and biodegradation of RSF, we believe that P(NIPAAm-*co*-AAc)/RSF fibrous

mats will show promising applications in controlled drug delivery, tissue engineering and biosensors.

Conflicts of interest

The authors declare there is no conflict of interest.

Acknowledgements

The authors acknowledge financial support from the Natural Science Foundation of Shanxi Province, China (201801D121102).

Notes and references

1 R. A. Siegel, *J. Controlled Release*, 2014, **190**, 337–351.
2 T. M. Reineke, *ACS Macro Lett.*, 2015, **5**, 14–18.
3 H. Chaobo, S. J. Soenen, R. Joanna, L. Bart, B. Kevin, D. Jo and S. C. De Smedt, *Chem. Soc. Rev.*, 2011, **40**, 2417–2434.
4 H. Li, K. Liu, G. R. Williams, J. Wu, J. Wu, H. Wang, S. Niu and L.-M. Zhu, *Colloids Surf., B*, 2018, **171**, 142–149.
5 J. Zhu, H. Han, T. Ye, F. Li, X. Wang, J. Yu and D. Wu, *Molecules*, 2018, **23**, 3383.
6 B. W. Li and H. C. Zeng, *Chem. Mater.*, 2019, **31**, 5320–5330.
7 A. Gandhi, A. Paul, S. O. Sen and K. K. Sen, *Asian J. Pharm. Sci.*, 2015, **10**, 99–107.
8 X. F. Sun, Q. Zeng, H. Wang and Y. Hao, *Cellulose*, 2018, **26**, 1909–1922.
9 S. S. Suradi, N. H. Naemuddin, S. Hashim and N. Adrus, *RSC Adv.*, 2018, **8**, 13423–13432.
10 G. Bokias, G. Staikos and I. Iliopoulos, *Polymer*, 2000, **41**, 7399–7405.
11 S. P. Rwei, W. Y. Chiang, T. F. Way, H. N. A. Tuan and Y. C. Chang, *Polymers*, 2018, **10**, 17.
12 R. Begum, J. Najeeb, G. Ahmad, W. Wu, A. Irfan, A. G. Al-Sehemi and Z. H. Farooqi, *React. Funct. Polym.*, 2018, **132**, 89–97.
13 X. Gao, C. Yue, X. Song, Z. Zhe, C. Xiao, C. He and X. Chen, *J. Mater. Chem. B*, 2013, **1**, 5578–5587.
14 Q. Wu, X. Tang, X. Liu, Y. Hou, H. Li, C. Yang, J. Yi, X. Song and G. Zhang, *Chem.–Asian J.*, 2016, **11**, 112–119.
15 J. Gan, X. Guan, J. Zheng, H. Guo, K. Wu, L. Liang and M. Lu, *RSC Adv.*, 2016, **6**, 32967–32978.
16 Z. Zhang, Y. Liu, X. Chen and Z. Shao, *RSC Adv.*, 2016, **6**, 48661–48665.
17 G. Zhen, T. T. Dang, M. Minglin, B. C. Tang, C. Hao, J. Shan, D. Yizhou, Z. Yunlong and D. G. Anderson, *ACS Nano*, 2013, **7**, 6758–6766.
18 L. Wang, X. Zhao, Y. Zhang, W. Zhang, T. Ren, Z. Chen, F. Wang and H. Yang, *RSC Adv.*, 2015, **5**, 40437–40443.
19 Y. Dong, X. Zhu, S. Feng and J. Nie, *Appl. Surf. Sci.*, 2014, **307**, 7–12.
20 R. Elashnikov, P. Slepička, S. Rimpelova, P. Ulbrich, V. Švorčík and O. Lyutakov, *Mater. Sci. Eng., C*, 2017, **72**, 293–300.
21 Y. Wang, C. Lai, H. Hu, Y. Liu, B. Fei and J. Xin, *RSC Adv.*, 2015, **5**, 51078–51085.
22 M. Chen, Y. F. Li and F. Besenbacher, *Adv. Healthcare Mater.*, 2015, **3**, 1721–1732.
23 X. Hu, S. Liu, G. Zhou, Y. Huang, Z. Xie and X. Jing, *J. Controlled Release*, 2014, **185**, 12–21.
24 P. Zhou, F. Zhou, B. Liu, Y. Zhao and X. Yuan, *J. Mater. Chem. B*, 2017, **5**, 9312–9325.
25 H. L. Zhou, Z. R. Shi, X. Wan, H. L. Fang, D. G. Yu, X. H. Chen and P. Liu, *Nanomaterials*, 2019, **9**, 14.
26 D. G. Yu, J. J. Li, G. R. Williams and M. Zhao, *J. Controlled Release*, 2018, **292**, 91–110.
27 D. G. Yu, M. L. Wang, X. Y. Li, X. K. Liu, L. M. Zhu and S. W. A. Bligh, *Wiley Interdiscip. Rev.: Nanomed. Nanobiotechnol.*, 2019, e1601, DOI: 10.1002/wnan.1601.
28 S. Fei, W. Xiu-Li and W. Yu-Zhong, *Colloids Surf., B*, 2011, **88**, 749–754.
29 Y. Kim, M. Ebara and T. Aoyagi, *Sci. Technol. Adv. Mater.*, 2012, **13**, 64203–64209.
30 H. Li, G. R. Williams, J. Wu, H. Wang, X. Sun and L. M. Zhu, *Mater. Sci. Eng., C*, 2017, **79**, 245–254.
31 F. Käfer, R. Vilensky, G. Vasilyev, E. Zussman and S. Agarwal, *Macromol. Mater. Eng.*, 2019, **304**, 1800606.
32 G. V Anand, R. Anupama Sargur, S. Radhakrishnan, R. Hemant Kumar, J. Sundaramurthy, S. Rahul, R. Seeram and B. Avinash, *Macromol. Rapid Commun.*, 2015, **36**, 1368–1373.
33 P. J. Sun, Y. H. Na, W. Dae Gyun, J. S. Yeon and P. Keun-Hong, *Biomaterials*, 2013, **34**, 8819–8834.
34 X. Jin, W. Qian, J. Sun, H. Panezail, W. Xia and S. Bai, *Polym. Bull.*, 2017, **74**, 3619–3638.
35 M. R. Islam, M. Tumbarello and L. A. Lyon, *Colloid Polym. Sci.*, 2019, **297**, 667–676.
36 H. Li, G. Zhang, L. Deng, R. Sun and O. Y. Xing, *RSC Adv.*, 2014, **5**, 6413–6418.
37 P. Slemming-Adamsen, S. Jie, M. Dong, F. Besenbacher and M. Chen, *Macromol. Mater. Eng.*, 2015, **300**, 1226–1231.
38 X. Lin, D. Tang, Z. Yu and F. Qian, *J. Mater. Chem. B*, 2014, **2**, 651–658.
39 W. Xiaoqin, Y. Tuna, L. Qiang, H. Xiao and D. L. Kaplan, *Biomaterials*, 2010, **31**, 1025–1035.
40 S. Yu, W. Yang, S. Chen, M. Chen and X. Chen, *RSC Adv.*, 2014, **4**, 18171–18177.
41 D. J. Hines and D. L. Kaplan, *Macromol. Chem. Phys.*, 2013, **214**, 280–294.
42 H. Li, J. Zhu, C. Song, J. Lan and Y. Ma, *RSC Adv.*, 2017, **7**, 56550–56558.
43 C. Vepari and D. L. Kaplan, *Prog. Polym. Sci.*, 2007, **32**, 991–1007.
44 J. Zhu, Y. Zhang, H. Shao and X. Hu, *Polymer*, 2008, **49**, 2880–2885.
45 H. Fong, I. Chun and D. H. Reneker, *Polymer*, 1999, **40**, 4585–4592.
46 D. N. Rockwood, D. B. Chase, R. E. Akins Jr and J. F. Rabolt, *Polymer*, 2008, **49**, 4025–4032.
47 A. R. Murphy and D. L. Kaplan, *J. Mater. Chem.*, 2009, **19**, 6443–6450.
48 H. Xiao, S. Karen, S. Lin, G. Eun-Seok, P. Sang-Hyug, C. Peggy and D. L. Kaplan, *Biomacromolecules*, 2011, **12**, 1686–1696.